A comprehensive reduced model of the mammalian cell cycle

Sofia Almeida, Madalena Chaves, Franck Delaunay, Celine Feillet

A comprehensive reduced model of the mammalian cell cycle

S. Almeida [*,**] **M. Chaves** [*] **F. Delaunay** [**] **C. Feillet** [**]

[*] *INRIA Sophia Antipolis, Université Côte d'Azur, France*
[**] *Université Côte d'Azur, CNRS, INSERM, iBV, France*
[***] *E-mails: sofia.almeida@inria.fr, madalena.chaves@inria.fr, franck.delaunay@unice.fr, celine.feillet@unice.fr*

Abstract:
The cellular division cycle is an essential process to ensure healthy tissue homeostasis, which can, due to its periodicity, be interpreted as a biological oscillator. This work focuses on identifying the main mechanisms underlying cell cycle rhythms in mammals and propose a mathematical model to describe them. The model is based on post-translational modifications of cyclin B-cdk1, also called mitosis promoting factor (MPF), known to be the essential protein of the mammalian cell cycle, as well as in its degradation by the APC:cdc20 complex. The final result is a two variable reduced model of the mammalian cell cycle that is able to reproduce oscillatory behaviors and properties consistent with observations, namely the period being tunable by an external input of growth factor. We calibrate and validate this model and study its behavior in a simple open-loop control configuration, showing that it can exhibit bistability and oscillations. The model presents an advantage to work with due to its low variable and parameter size.

Keywords: Cell Cycle, biological oscillator, tunable period, open-loop control, bistability

1. INTRODUCTION

The cycle of life of eukaryotic cells is under tight control of a vast network of regulatory molecular processes in order to ensure that the cells grow, proliferate and die at proper rhythms and in a manner consistent with cellular health maintenance. As such, the cell cycle is a key process involved in DNA synthesis and repair, cellular differentiation and programmed cell death, making it one of the most essential mechanisms to life. Uncontrolled cell proliferation on the other hand is characteristic of cancer, thus understanding and controlling the cell cycle is of the utmost importance in cancer treatment.

The cell cycle occurs rhythmically resulting in a periodic oscillation of protein levels and activity, gene activation patterns and cellular morphology: it produces a biorhythm and can thus be interpreted as an oscillator. The cell cycle of several mammalian cells has a period of approximately 24 h and is coupled to the cellular circadian clock, another important biological oscillator, see Feillet et al. (2014) and Feillet et al. (2015). Furthermore, the rate of division in a culture of mammalian cells varies accordingly with the amount of "growth factors", which are represented by a specific class of peptidic hormones added to the medium, allowing to tune the period of the oscillator.

Mathematical modeling has become particularly instrumental to study the cell cycle due to the increasingly known complexity of molecular controls involved in the process, see Sible and Tyson (2007). Models have become a powerful tool to study cell division systems, investigate the core mechanisms behind cell cycle rhythms and make predictions. Novak and Tyson (1993), Gérard and Goldbeter (2009), Pomerening et al. (2003) and Gérard and Goldbeter (2011) are successful examples of reference models for the mammalian cell cycle that vary in complexity and approach. The drawback of these models is their size which prevents analytical study of the parameter space in order to explore the various dynamical regimes.

With the goal of studying the main circuits underlying cell cycle rhythms and prove existence of oscillations and other properties we develop a reduced variable mechanistic model of ordinary differential equations (ODE) based on MPF (mitosis promoting factor, the cyclin B:cdk1 complex) which is the active component of the G2 phase that is known to be necessary and sufficient to carry out the mitotic process (as seen in Ciliberto et al. (2005) and Novak and Tyson (1993)).

The model proposed here includes phosphorylation and dephosphorylation steps carried out between MPF, wee1 and cdc25 (Perry and Kornbluth (2007)) responsible for positive feedback-loops on MPF, as well as degradation of MPF by the APC:cdc20 complex (Kramer et al. (2000)) forming a negative feedback loop. While negative feedback loops are essential for oscillation, the positive feedback-loops allow to tune the period of systems without compromising the amplitude of the signal, see Tsai et al. (2008). The MPF/APC:cdc20 feedback loop has also been previously studied and modeled, see Gérard et al. (2015), Yang and Ferrell (2013).

Section 2 presents an intermediate-sized model, based on the reference mechanisms already described in Novak and Tyson (1993) and Gérard et al. (2015). This model is then reduced to a 2D model (section 3) containing all the

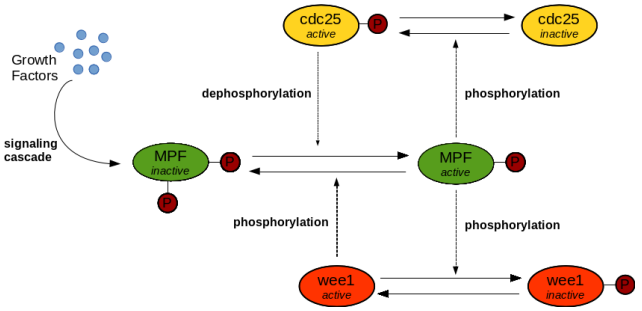

Fig. 1. Schematic representation of the positive feedback loop between MPF and cdc25 and of the double-negative feedback loop of MPF with wee1.

mechanisms and is calibrated against cyclin B-cdk1 data Pomerening et al. (2005) in order to obtain a physiological parameter set. Finally, in section 4 we present a numerical and analytical analysis of the parameter space, we observe that the 2D model captures well the period variation with growth factor and study a scenario of bifurcation between bistability and oscillations.

2. A 7D INTERMEDIATE MODEL

To obtain a low dimension model of the cell cycle, we first develop and then reduce an intermediate model.

First, the schematic of Fig. 1 summarizes some main processes responsible for MPF activation and inactivation. The inactive form of MPF has an extra phosphate group relative to the active one; cdc25 is a kinase responsible for removing this phosphate group leading to the activation of the MPF while wee1 is a kinase that phosphorylates MPF promoting its inactive form, Perry and Kornbluth (2007). Furthermore, MPF itself phosphorylates cdc25 activating it and forming a positive feedback-loop, as well as phosphorylating wee1 and inactivating it, forming a double-negative feedback loop, that acts as a positive loop.

Here, we consider that there is no production or destruction of cdc25 and wee1, meaning $[cdc25_{inactive}] = cdc25_{TOT} - [cdc25]$ and $[wee1_{inactive}] = wee1_{TOT} - [wee1]$, where $cdc25_{TOT}$ and $wee1_{TOT}$ are total amounts. Equations (1) to (4) model these processes.

The growth factor GF binds to receptors of the cellular membrane and initiates a signalling cascade that leads to the production of cyclin B, here represented by a synthesis term S_{GF} in equation (4) given by $S_{GF} = V_f \frac{GF^n}{GF^n + k_f^n}$. If GF is constant, so is S_{GF} and we assume that S_{GF} is a direct representation of the input.

$$\frac{d[cdc25]}{dt} = V_1 \frac{cdc25_{TOT} - [cdc25]}{cdc25_{TOT} - [cdc25] + k_1}[MPF] - V_2 \frac{[cdc25]}{[cdc25] + k_2} \quad (1)$$

$$\frac{d[wee1]}{dt} = V_3 \frac{wee1_{TOT} - [wee1]}{wee1_{TOT} - [wee1] + k_3} - V_4 \frac{[wee1]}{[wee1] + k_4}[MPF] \quad (2)$$

$$\begin{aligned}\frac{d[MPF]}{dt} =& V_5 \frac{[MPF_{inactive}]}{[MPF_{inactive}] + k_5}[cdc25] - V_6 \frac{[MPF]}{[MPF] + k_6}[wee1] \\ & - \gamma_1 [APC : cdc20][MPF]\end{aligned} \quad (3)$$

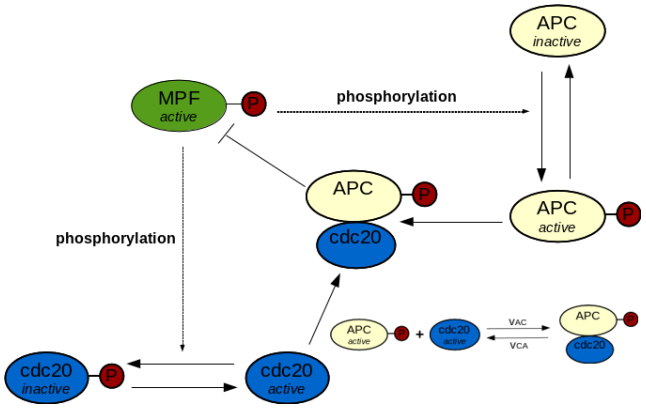

Fig. 2. Schematic representation of the negative feedback loop between MPF and the APC:cdc20 complex: MPF promotes the formation of APC:cdc20 by activating APC, while APC:cdc20 represses MPF by degradation. The APC:cdc20 complex can also dissociate.

$$\begin{aligned}\frac{d[MPF_{inactive}]}{dt} =& S_{GF} - V5 \frac{[MPF_{inactive}]}{[MPF_{inactive}] + k_5}[cdc25] \\ & + V_6 \frac{[MPF]}{[MPF] + k_6}[wee1] \\ & - \gamma_2 [APC : cdc20][MPF_{inactive}]\end{aligned} \quad (4)$$

The second part of the model is represented in the scheme of Fig. 2 and describes the degradation of MPF by the complex APC:cdc20. These two components form a negative feedback-loop, with MPF phosphorylating the anaphase-promoting complex APC, leading it to a configuration that will dimerize with cdc20. The APC:cdc20 complex promotes the ubiquitination of MPF, targetting it for degradation. MPF has an opposite effect on cdc20 causing its inactivation and we include this step on the model as a first approach. The complex APC:cdc20 can dissociate into cdc20 and APC, see Fig. 2. Once more, we consider that there is no synthesis or degradation of cdc20 and APC, which allows us to write $[APC_{inactive}] = APC_{TOT} - [APC] - [APC : cdc20]$ and $[cdc20_{inactive}] = cdc20_{TOT} - [cdc20] - [APC : cdc20]$. Equations (5) to (7) model these steps.

$$\begin{aligned}\frac{d[APC]}{dt} =& V_7 \frac{APC_{TOT} - [APC] - [APC : cdc20]}{APC_{TOT} - [APC] - [APC : cdc20] + k_7}[MPF] \\ & - V_8 \frac{[APC]}{[APC] + k_8} - v_{AC}[APC][cdc20] + \\ & v_{CA}[APC : cdc20]\end{aligned} \quad (5)$$

$$\begin{aligned}\frac{d[cdc20]}{dt} =& V_9 \frac{cdc20_{TOT} - [cdc20] - [APC : cdc20]}{cdc20_{TOT} - [cdc20] - [APC : cdc20] + k_9} \\ & - V_{10} \frac{[cdc20]}{[cdc20] + k_{10}}[MPF] - v_{AC}[APC][cdc20] \\ & + v_{CA}[APC : cdc20]\end{aligned} \quad (6)$$

$$\frac{d[APC : cdc20]}{dt} = v_{AC}[APC][cdc20] - v_{CA}[APC : cdc20] \quad (7)$$

This model has an oscillatory behavior as shown in Fig. 3, for representative parameters. A calibration of the parameters is shown below for the reduced model. We also verify the tunability of the period with the input S_{GF},

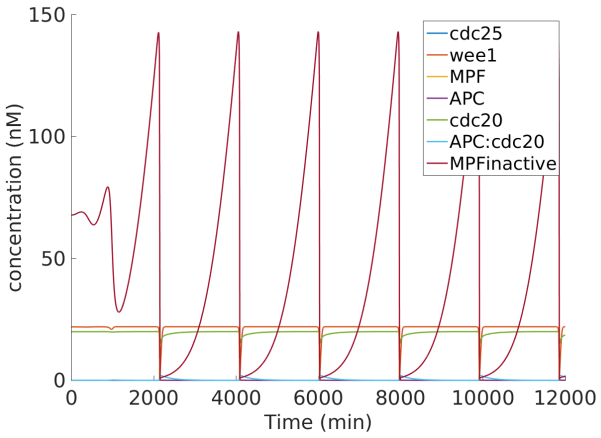

Fig. 3. Oscillations of the components of the cell cycle model. Parameters: $wee1_{TOT} = 22.0$, $cdc25_{TOT} = 20.0$, $APC_{TOT} = 40.0$, $cdc20_{TOT} = 20.0$, $\gamma_1 = 3.0$, $\gamma 2 = 0.1$, $V_1 = 0.1$, $k_1 = 7.6$, $V_2 = 2.5$, $k_2 = 7.6$, $V_3 = 0.5$, $k_3 = 5.4$, $V_4 = 5.0$, $k_4 = 4.3$, $V_5 = 70.0$, $k_5 = 50.0$, $V_6 = 20.0$, $k_6 = 50.0$,$V_7 = 0.1$, $k_7 = 10.2$, $V_8 = 1.0$, $k_8 = 10.5$, $V_9 = 1.5$, $k_9 = 50.6$, $V_{10} = 0.5$, $k_{10} = 60.1$, $V_{AC} = 0.2$, $V_{CA} = 0.15$ and $S_{GF} = 0.24$. Units for V_1, V_4, V_5, V_6, V_7, V_{10} and V_{CA} are min^{-1} for V_2, V_3, V_8, V_9 and S_{GF} are $nM.min^{-1}$, for γ_1, γ_2 and V_{AC} are $min^{-1}.nM^{-1}$ and for all $k's$ are nM.

for example for $S_{GF} = 0.24\ nmol.min^{-1}$, $T = 1942\ min$ and for $S_{GF} = 2.0\ nmol.min^{-1}$, $T = 1139\ min$. We verify that our total amounts of concentrations are close to those obtained by Pomerening et al. (2005) and we chose the units of our preliminary parameters based on that work. This model can be interpret in relation to the cell cycle with the peaks of MPF corresponding to mitosis and the times when wee1 is high as the remaining phases of the cell-cycle preceeding mitosis.

3. MODEL REDUCTION AND CALIBRATION

The model has relaxation oscillations with certain variables varying through plateaus (see Fig. 3), thus in order to reduce it we start by setting cdc25 and wee1 at steady-state, i.e. $\frac{dx_i}{dt} = 0$ with x_i representing a generic variable. This results in:

$$MPF(cdc25) = \frac{V_2}{V_1}\frac{[cdc25]}{[cdc25]+k_2}\frac{cdc25_{TOT}-[cdc25]+k_1}{cdc25_{TOT}-[cdc25]} \tag{8}$$

and

$$MPF(wee1) = \frac{V_3}{V_4}\frac{wee1_{TOT}-[wee1]}{wee1_{TOT}-[wee1]+k_3}\frac{[wee1]+k_4}{[wee1]} \tag{9}$$

We want to replace the variables cdc25 and wee1 in equation (3) by a term dependent on MPF, thus we invert the functions given by equations (8) and (9) and verify that the inverse functions can be well approximated by Hill functions, as follows:

$$cdc25(MPF) = cdc25_{TOT}\frac{[MPF]^m}{[MPF]^m + k_m^m} \tag{10}$$

and

$$wee1(MPF) = wee1_{TOT}\frac{k_n^n}{[MPF]^n + k_n^n} \tag{11}$$

where the cdc25 equation (10) is that of an activator or promoter and wee1 equation (11) represents a repressor.

Next, we observe that cdc20 isn't an essential variable for the oscillary behavior and we can make it constant.

Now focusing on the APC equation, we study the variations on parameters in equation (5). We verify that the parameter k_7 can be decreased to very low values without changing the output of the model: $k_7 \simeq 0$, implying that the first Michaelis-Menten term of equation (5) is saturated and can be approximated by a constant. Furthermore, we also verify that almost all the time $k_8 > [APC]$ and k_8 can be very large without dramatically affecting the system, which in its turn implies that the second Michaelis-Menten term of equation (5) can be approximated by a linear function. Thus,the equation for APC becomes:

$$\begin{aligned}\frac{d[APC]}{dt} =& V_7[MPF] - \frac{V_8}{k_8}[APC] - v_{AC}[APC][cdc20] \\ &+ v_{CA}[APC:cdc20]\end{aligned} \tag{12}$$

Now we put APC at steady-state to obtain:

$$[APC] = \frac{V_7[MPF] + v_{CA}[APC:cdc20]}{v_{AC} + \frac{V_8}{k_8}} \tag{13}$$

substituting in equation (7), leads to:

$$\frac{d[APC:cdc20]}{dt} = V_m[MPF] - V_k[APC:cdc20] \tag{14}$$

with parameters

$V_m = \frac{v_{AC}V_7}{v_{AC}+\frac{V_8}{k_8}}$ and $V_k = v_{CA}(1 - \frac{v_{AC}}{v_{AC}+\frac{V_8}{k_8}})$.

Lastly, we procceed to merge the two MPF equations (3 and 4). We look to remove the equation for $MPF_{inactive}$ as well as keeping Michaelis-Menten terms in the final equation to represent the phosphorylation and dephosphorylation of MPF, in coherence with the previous model. We verify that for non-negligible values of S_{GF} enough $MPF_{inactive}$ is created so that the production of MPF is never compromised. Thus, we consider an average maximum amount $\overline{MPF_{max}}$ from where we can define $MPF_{inactive} = \overline{MPF_{max}} - MPF$. The parameter $\overline{MPF_{max}}$ doesn't represent a total amount of MPF since there is also a production term S_{GF}. In section 4.2 we will include the effect of S_{GF} on the total amount of MPF.

In equation (15) we observe the simplified MPF reduced equation, which also contains the growth factor input:

$$\begin{aligned}\frac{d[MPF]}{dt} =& S_{GF} + V_c\frac{\overline{MPF_{max}} - [MPF]}{\overline{MPF_{max}} - [MPF] + k_c}\frac{[MPF]^m}{[MPF]^m + k_m^m} \\ &- V_w\frac{[MPF]}{[MPF]+k_w}\frac{k^n}{[MPF]^n + k_n^n} \\ &- \gamma_1[APC:cdc20][MPF]\end{aligned} \tag{15}$$

The exponents m and n take the value of 2 and V_c and V_w represent $V_5 cdc25_{TOT}$ and $V_6 wee1_{TOT}$ respectively (see

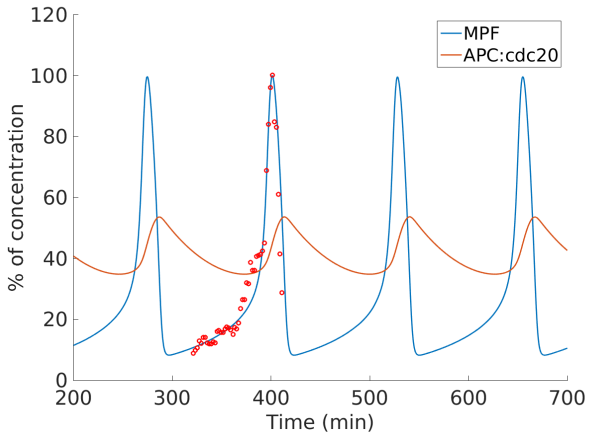

Fig. 4. Oscillations of MPF and APC:cdc20 over time. Adjustment of the model to data points nomalized to 100, retrieved from Pomerening et al. (2005). Obtained parameters are presented in Table 1.

equations (3), (10) and (11)).The $APC : cdc20$ complex is as given by equation (14).

Our final model is thus given by equations (15) and (14). The numerical simulations give again rise to relaxation oscillations as observed in Fig. 4 (period 126.8 min), with the peaks of MPF indicating mitosis. Parameters are presented in Table 1 and were obtained through adjustment to data points by means of a computational optimization, see Fig. 4. Data points for calibration were collected from Pomerening et al. (2005) that presents experimental results of normalized cyclin levels and cdc2 activity for the Xenopus egg.

Table 1. Calibrated parameters

p	Numerical Value
γ_1	0.0162 min^{-1}
V_c	225.71 min^{-1}
k_c	130.3331
V_w	747.61 min^{-1}
k_w	137.9830
k_m	98.5219
k_n	0.1164
V_m	0.0168 min^{-1}
V_k	0.0107 min^{-1}
S_{GF}	5.6917 min^{-1}
$\overline{MPF_{max}}$	284.1087

It is clear that our model faithfully represents the dynamics of cyclin B, with a set of physiological parameters that leads to oscillatory behavior. The fact that the reduced model again produces relaxation oscillations for MPF as well as tuning of the period through GF (see section 4.2), allows us to consider that the essential mechanistic steps of our first model are conserved.

4. MATHEMATICAL ANALYSIS

Next, we analyse how oscillations are originated by an unstable fixed-point inside a limited phase-plane region. The nullclines are shown in Fig. 6. As discussed before, $\overline{MPF_{max}}$ will be an approximate limit for the maximum value of MPF, which in its turn will limit the amount of APC:cdc20, thus forming a foward-invariant region for

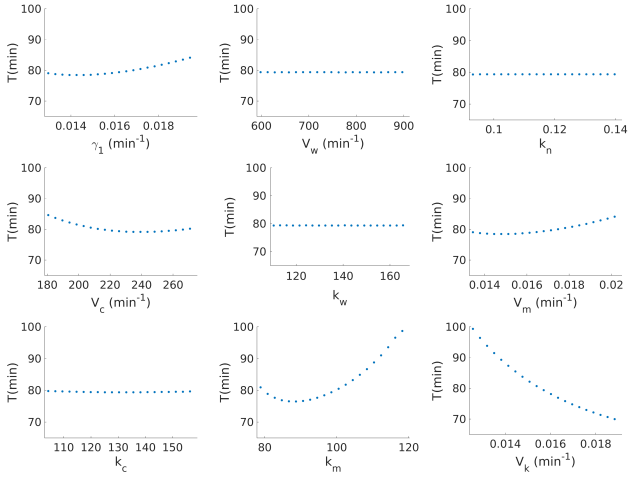

Fig. 5. Sensitivity analysis of the model. Parameters are varied 20 % around a value in the middle of the oscillation region - (Table 1, with $V_k = 0.0157\ min^{-1}$).

this system. Inside this region there is a unique fixed point, which is unstable when the two nullclines intersect in an interval where both are increasing. For this set of parameters, the nullclines intersect at $(23.03, 36.16)$ and this is an unstable fixed point. Under these conditions, applying the Poincaré-Bendixson Theorem to this 2D system proves the existence of a periodic orbit.

The rate of production of the APC:cdc20 complex by MPF (V_m) and the natural degradation of APC:cdc20 (V_k) control the slope of the APC:cdc20 nullcline. For the parameters of Table 1 the nullclines intersect near the beginning of the oscillatory region (Fig. 6), however the calibration with data for the Xenopus egg gives us mostly the order of magnitude for the parameters of a mammalian cell, thus we can change slightly the value of V_k in order to have a broader study of the parameters in the oscillatory region in Fig. 5. From observation of Fig. 5 we can conclude that V_m, V_k and k_m are the parameters that produce greater changes in the period and that overall the system is robust for parameters.

4.1 Parameters Analytical Characterization

In order to obtain broader limits for the parameters than those that numerical simulations allow and to better understand how each term of the model equations affects the dynamics, we analyse possible relations between parameters that can guarantee existence of oscillation.

From the observed dynamics of our oscillations (Fig. 6), we require the MPF nullcline to be increasing when it intersects with the APC:cdc20 nullcline in order to obtain an unstable fixed-point. Thus, we consider now the MPF nullcline as $g_1(x)$ and the APC:cdc20 nullcline as $g_2(x)$, represented in equations (16) and (17), with $\overline{MPF_{max}}$ now called X_M for simplicity:

$$g_1(x) = \frac{S_{GF}}{\gamma_1 x} + \frac{V_c}{\gamma_1 x}\frac{X_M - x}{X_M - x + k_c}\frac{x^2}{x^2 + k_m^2} - \frac{V_w}{\gamma_1 x}\frac{x}{x + k_w}\frac{k^2}{x^2 + k_n^2} \tag{16}$$

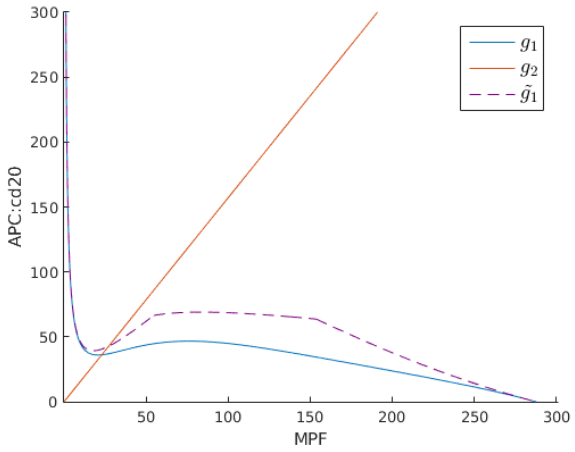

Fig. 6. Blue curve (g_1): MPF nullcline, red curve (g_2): APC:cdc20 nullcline (parameters given in Table 1), dashed purple curve ($\tilde{g}_1$): piecewise quadratic approximation of the MPF nullcline.

$$g_2(x) = \frac{Vm}{Vk}x \tag{17}$$

and determine the local minimum and maximum points x_1 and x_2 that will delimit the region of increasing g_1. The intersection point of g_1 and g_2 must satisfy $\frac{g_1(x_2)}{x_2} < \frac{V_m}{V_k} < \frac{g_1(x_1)}{x_1}$ (see equation 17) in order for the nullclines to intersect in the growing region of g_1. For the set of calibrated parameters (Table 1) we determine x_1 and x_2 numerically and verify $0.61 < \frac{V_m}{V_k} < 1.73$.

We now proceed to approximate the terms of $g_1(x)$ by piecewise quadratic functions. For example, considering $h_1(x)$ as the activator Hill function in equation (16) we design an approximation given by:

$$h_1(x) = \frac{x^2}{x^2 + k_m^2} = \begin{cases} \alpha x^2 & \text{if } x < x_a \\ -a(x - X_M)^2 + h_1(X_M) & \text{if } x_a < x < X_M \end{cases}$$

We choose $\alpha = 8.10^{-7}k_m$ in order to define a quadratic function that approximates well the first region of h_1, $x_a = \sqrt{\frac{1-\alpha k m^2}{\alpha}}$ is the point where the function intersects h_1. The second equation defines an inverted parabola whose maximum is set at X_M, with a defined as $a = \frac{h_1(X_M)+\alpha k m^2 - 1}{(x_a - X_M)^2} > 0$ in order to have continuity at x_a.

The space is split into five intervals: $0 < x < \sqrt{2}k_n$, $\sqrt{2}k_n < x < x_a$, $x_a < x < k_w$, $k_w < x < X_M - k_c$ and $X_M - k_c < x < X_M$ that define the limits of the piecewise quadratic approximation $\tilde{g}_1$ (shown in Fig. 6).

Intervals 2 and 3 contain the region where the function increases (Fig. 6), at these intervals $\tilde{g}_1$ is defined as:

$$\tilde{g}_1^2(x) = \frac{S_{GF}}{\gamma_1 x} + V_c \alpha x \tag{18}$$

$$\tilde{g}_1^3(x) = \frac{1}{\gamma_1 x}[S_{GF} + V_c(-a(x - X_M)^2 + h_1(X_M))] \tag{19}$$

The derivative of $\tilde{g}_1^2(x)$ has a zero at $\tilde{x}_1 = \sqrt{\frac{S_{GF}}{\alpha V_c}}$ that marks the begining of the increasing region, the derivative of $\tilde{g}_1^3(x)$ as a zero at $\tilde{x}_2 = \sqrt{\frac{V_c(aX_M^2 - h_1(X_M)) - S_{GF}}{aV_c}}$ that limits the upper bound of the interval. Thus, in a broad manner we may conclude that the parameters need to satisfy $\tilde{x}_1 < \tilde{x}_2$, or:

$$S_{GF} < V_c \frac{\alpha(aX_M^2 - h_1(X_M))}{a + \alpha} \tag{20}$$

which we can interpret as giving the maximum value of the growth-factor dependent synthesis term S_{GF} in relation to V_c that guarantees oscillations. S_{GF} and V_c together account for the total production of MPF in the model, with V_c being the maximum value of the positive Michaelis-Mentem term (representing formation of MPF from $MPF_{inactive}$) in equation (15), this allows us to conclude that the limit of growth factor above which oscillations stop is dependent on the rate of MPF phosphorylation by cdc25. Using the parameters presented in Table 1 and the mentioned value of α we obtain $S_{GF} < 21.6105$ and verify the condition (20).

The piecewise quadratic approximation shows that an interval where $g_1([MPF])$ increases appears due to a dominance of the Hill term coming from the cdc25 positive loop, $V_c \frac{MPF^2}{MPF^2 + k_m^2}$. It furthermore captures the properties needed to generate sustained oscillations, yielding relations between the parameters that allow to characterize the oscillatory behavior.

4.2 Open-loop Control and Bistability

In Fig. 7 we can see that the model reproduces the trend of period tunable with a Growth Factor input, where an adjustment is made between our output and experimental data from Table 2. The experimental data points come mostly from Feillet et al. (2014), with the exception of the 5% FBS (fetal bovine serum) value, that is an additional measurement done under the exact same experimental conditions (unperturbed NIH 3T3 mouse fibroblasts). We do a scaling in our model such as $t \to \beta t$, which leads to $S_{GF} \to \frac{S_{GF}}{\beta}$, with $\beta = 0.1$.

Table 2. Experimental data for the period tunable with GF (Feillet et al. (2014))

$\%FBS$	$T(h)$
5	26.6
10	21.3
15	18.6
20	16.5

Lastly, seeking to improve the approximation made in section 3 as: $MPF_{inactive} = \overline{MPF_{max}} - MPF$, we study the case in which $\overline{MPF_{max}}$ also depends on the input: $\overline{MPF_{max}} = \overline{MPF_{max}} + \beta S_G F$ in equation (15). This recovers a property of our 7D model in which S_{GF} will have an effect in the amount of $MPF_{inactive}$ available to generate MPF.

An interesting result is that for certain values of $\overline{MPF_{max}}$, the model switches from the oscillatory regime to a bistable regime as the input S_{GF} increases. Fig. 8 presents

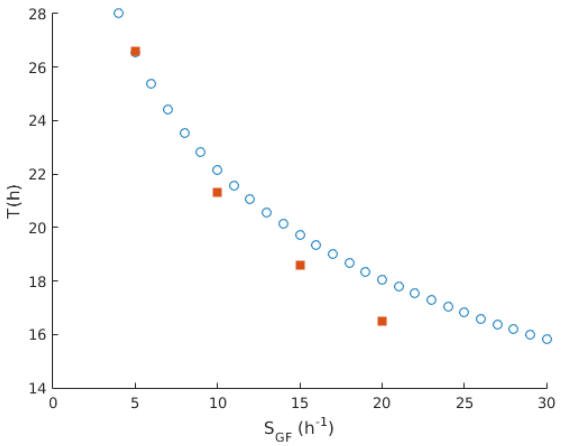

Fig. 7. Period tunable with the input S_{GF}: open-loop control. We do a scaling correspondance of our numerical simulations (blue circles) with data from Table 2 (red squares).

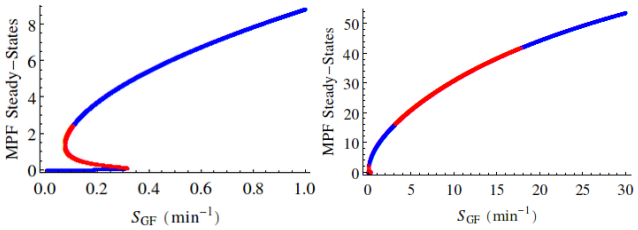

Fig. 8. MPF steady-states as a function of the parameter S_{GF}, left side of image shows a zoom for S_{GF} between 0 and 1. Stable steady states are represented in blue and unstable steady-states in red.

the MPF steady states for different values of S_{GF}, with $\overline{MPF_{max}} = 150$ and $\beta = 20$. We can observe, with increasing S_{GF}, the passage from a monostable regime to bistability, to again monostability, then entering the oscillation region with one unstable fixed point and finally monostability again. The entrance in the oscillatory region is marked by a Hopf bifurcation.

The input parameter S_{GF} controls the change between dynamic regimes and we can delimit the oscillatory regime for 3.3 $min^{-1} < S_{GF} < 17.7\ min^{-1}$.

From a biological point of view this raises the question of whether cells grown with low growth factor and unable to divide would present bistability. Bistability in the activation of cdc2 has been observed by Pomerening et al. (2003) on a modified system.

5. CONCLUSION

A two variable cell cycle model based on the negative feedback loop between MPF and the APC:cdc20 complex and on a positive feedback loop of MPF was calibrated from experimental data for cyclin B from one study (Pomerening et al. (2005)) and was able to reproduce experimental data from another study (Feillet et al. (2014)) for the tunability of the period with the growth factor input.

The growth factor input controls the output of the system determining switching behavior between bistability, monostability and oscillations. The cell cycle is understood in terms of relations between parameters representing the G2 phase, with the activity of cdc25 being dominant over the other components, producing the biorhythm.

ACKNOWLEDGEMENTS

The authors are part of the Labex SIGNALIFE Network for Innovation on signal Transduction Pathways in Life Sciences (Grant ANR-11-LABX-0028-01), ANRHyClock project (ANR-14-CE09-0011) and iCycle project (ANR-16-CE33-0016-01).

REFERENCES

Ciliberto, A., Lukács, A., Tóth, A., Tyson, J., and Novák, B. (2005). Rewiring the exit from mitosis. *Cell Cycle*, 4(8), 1107–1112.

Feillet, C., Krusche, P., Tamanini, F., Janssens, R., Downey, M., Martin, P., Teboul, M., Saito, S., Lévi, F., Bretschneider, T., van der Horst, G., Delaunay, F., and Rand, D. (2014). Phase locking and multiple oscillating attractors for the coupled mammalian clock and cell cycle. *Proc Natl Acad Sci U S A*, 111(27), 9828–9833.

Feillet, C., van der Horst, G., Levi, F., Rand, D., and Delaunay, F. (2015). Coupling between the circadian clock and cell cycle oscillators: Implication for healthy cells and malignant growth. *Front Neurol.*, 11;6:96.

Gérard, C. and Goldbeter, A. (2009). Temporal self-organization of the cyclin/cdk network driving the mammalian cell cycle. *Proc. Natl. Acad Sci U.S.A*, 106(51), 21643–21648.

Gérard, C. and Goldbeter, A. (2011). A skeleton model for the network of cyclin-dependent kinases driving the mammalian cell cycle. *Interface Focus*, 1(1), 24–35.

Gérard, C., Tyson, J., Coudreuse, D., and Novák, B. (2015). Cell cycle control by a minimal cdk network. *PLoS Comput Biol*, 11(2).

Kramer, E., Scheuringer, N., Podtelejnikov, A., Mann, M., and Peters, J. (2000). Mitotic regulation of the apc activator proteins cdc20 and cdh1. *Mol Biol Cell*, 11(5), 1555–1569.

Novak, B. and Tyson, J. (1993). Numerical analysis of a comprehensive model of m-phase control in xenopus oocyte extracts and intact embryos. *J Cell Sci*, 106, 1153 – 1168.

Perry, J. and Kornbluth, S. (2007). Cdc25 and wee1: analogous opposites? *Cell Div.*

Pomerening, J., Kim, S., and Ferrell, J.J. (2005). Systems-level dissection of the cell-cycle oscillator: bypassing positive feedback produces damped oscillations. *Cell*, 122(4), 565–578.

Pomerening, J., Sontag, E., and Ferrell, J.J. (2003). Building a cell cycle oscillator: hysteresis and bistability in the activation of cdc2. *Nat Cell Biol*, 5(4), 346–351.

Sible, J. and Tyson, J. (2007). Mathematical modeling as a tool for investigating cell cycle control networks. *Methods*, 41(2), 238 – 247.

Tsai, T.Y.C., Choi, Y.S., Ma, W., Pomerening, J.R., Tang, C., and Ferrell, J.E.J. (2008). Robust, tunable biological oscillations from interlinked positive and negative feedback loops. *Science*, 321, 126–129.

Yang, Q. and Ferrell, J.J. (2013). The cdk1-apc/c cell cycle oscillator circuit functions as a time-delayed, ultrasensitive switch. *Nat Cell Biol*, 15(5), 519–525.